Mechanical Superheterodyne and Its Use for Low Frequency Vibrations Sensing

Naftaly Krakover, Ronen Maimon, Tamar Tepper-Faran, Yuval Gerson, Richard Rand, and Slava Krylov, *Senior Member, IEEE*

***Abstract*— Mechanical micro and nano scale devices are being increasingly used for realizing signal processing and logic or computing functions, which until recently were traditionally performed by electronics. Extremely low-power consumption and robustness make mechanical micro structures attractive for implementation in autonomous distributed sensing systems. Heterodyning is one of the most important and indispensable signal processing techniques. In microelectromechanical heterodynes, the frequency mixing is commonly achieved using nonlinear forces, which often limits scalability and the operational range of the device and may lead to undesired dynamic behavior. In this paper, we introduce an approach allowing purely mechanical realization of the superheterodyne principle. The frequency mixing is based on the inertial coupling between two vibratory modes of the device. The architecture is distinguished by linearity of the mixing term with respect to the input inertial and the local oscillator signals. We demonstrate the mixing effect both theoretically and experimentally, using the devices fabricated from a silicon on insulator (SOI) wafer by deep reactive ion etching (DRIE). We show the applicability of the device as a mechanical low frequency vibration sensor. The substrate vibration frequencies down to 25 Hz were measured using a device with a fundamental mode frequency of 4700 Hz.**

***Index Terms*— Heterodyne, vibrations sensing, variable inertia, inertial coupling, mechanical signal processing.**

I. Introduction

HETERODYNING is one of the key elements in modern signal processing [1]. This technique permits mixing of two signals with different frequencies ω_1 and ω_2 to produce two new signals with the frequencies $\omega_1 - \omega_2$ and $\omega_1 + \omega_2$. This principle is implemented in countless applications, for example, radio and optical [2] communication, frequency measurements [3] and high precision optical detection [4]. Heterodyning is routinely realized using electronic elements operated in a nonlinear regime [5].

Advances in micro- and nanotechnology opened new opportunities in design and operation of extremely downscaled machines with previously unthinkable performance. This stimulated a renewed interest to (electro-)mechanical realization of various signal processing functions, which in the past were reserved solely for electronics. Micro- and nanoelectromechanical systems (MEMS/NEMS) were successfully implemented not only as analog radio frequency (RF) components such as filters [6], multiplexers [7], counters [8] and frequency control and timing devices [9], but also as micro mechanical memories [10] and logic elements [11], [12]. While their penetration into the electronic components market is still low, mechanical devices offer unique functional advantages making them attractive. Resonant micro- and nanomechanical structures often exhibit smaller losses, lower power consumption, wider operational range and better frequency stability than their electronic counterparts, while preserving comparable size and 1 operational frequencies [9], [13].

Emerging of new technologies, such as Internet of Things (IoT) or wearables for personalized health care, both essentially based on distributed data collecting networks, imposes new demanding power consumption, integrability and overall size requirements to the sensing systems. The use of mechanical structures serving simultaneously as a sensing element and as a logic data processing device may reduce or even eliminate the need in electronic data processing, therefore reducing dissipated power to minimum. As an example, one can mention threshold inertial switches [14] or contact-based vibration detectors for wireless wake-up monitoring sensors, [15] both serving as mechanical alternatives to the computationally intensive post-processing of the time history data collected by accelerometers. In addition, mechanical structures are generally less prone to the electromagnetic interference (EMI) and can be operated in harsh environments such as elevated temperatures or radioactivity [16]. Within the long standing arena of analog computing, [17], [18] mechanical devices are considered as one of the possible approaches, which may pave the way to zero power reversible computing [19].

Similarly to mechanical computing, the idea of mechanical heterodyne has a long history. Complex macro-scale mechanisms realizing the heterodyne principle were already reported back in the sixties [20]. At the micro- and nanoscale, electromechanical MEMS/NEMS heterodynes reported so far exploited nonlinear electrostatic [21]–[27], electro

Manuscript received September 20, 2018; revised January 6, 2019; accepted February 23, 2019. Date of publication March 27, 2019; date of current version May 31, 2019. This work was supported by RAFAEL. The work of R. Rand was supported by the National Science Foundation under Grant CMMI-1634664. The work of S. Krylov was supported by the Henry and Dinah Krongold Chair of Microelectronics. Subject Editor A. Seshia. *(Naftaly Krakover and Ronen Maimon contributed equally to this work.) (Corresponding author: Naftaly Krakover.)*

N. Krakover, Y. Gerson, and S. Krylov are with the School of Mechanical Engineering, Faculty of Engineering, Tel Aviv University, Tel Aviv 69978, Israel (e-mail: naftalyk@mail.tau.ac.il; yoval.gerson@gmail.com; vadis@eng.tau.ac.il).

R. Maimon and T. Tepper-Faran are with the MANOR A.D.T. Division, Rafael Advanced Defense Systems Ltd., Haifa 31021, Israel (e-mail: ronenma12@gmail.com; tamarte@rafael.co.il).

R. Rand is with the Department of Mathematics, Sibley School of Mechanical and Aerospace Engineering, Cornell University, Ithaca, NY 14853 USA (e-mail: rrand@cornell.edu).

This paper has supplementary downloadable material available at http://ieeexplore.ieee.org, provided by the author.

Color versions of one or more of the figures in this paper are available online at http://ieeexplore.ieee.org.

Digital Object Identifier 10.1109/JMEMS.2019.2903265

thermal [28] or optical [29] forces to serve as a frequency multiplying element. For example, the intrinsic structure of the electrostatic forces $F_e = V^2(t)\mathcal{G}(u)$, where $V(t)$ is a time-dependent voltage and $\mathcal{G}(u)$ is a nonlinear function of the device's response $u(t)$, allows mixing by means of multi-frequency excitation, when $V = V_1\cos(\omega_1 t) + V_2\cos(\omega_2 t)$ [21]–[25]. A superheterodyne device, which exploits an electrostatic coupling between the different parts of the multi degrees of freedom (DOF) structure, each vibrating at different frequencies, was reported in [30] and [31]. Linearity of the frequency multiplying term was achieved by implementing a comb drive transducer with linearly varying electrodes length. In all of these cases, the heterodyning effect is based on the nature of the actuation forces, rather than on mechanical effects.

Here we report on an approach allowing purely mechanical realization of the superheterodyne principle. The device is based on the inertial geometric coupling (it is to say, the coupling appearing due to the changes in the device geometry influencing the inertial terms) between the translational and tilting vibrational modes of a proof mass attached to an oscillating substrate. In our architecture, the translational vibration creates a time-harmonic offset between the centroid of the proof mass and the tilting axis. As a result, the actuating moment driving the tilting vibrations and serving as the frequency mixing element emerges as a product between the inertial force associated with the substrate acceleration and the time-harmonic translational displacement. In other words, the translational motion serves as a local oscillator providing a carrier signal, whereas the tilting mode vibrations are excited at a fixed intermediate frequency.

We demonstrate, both theoretically and experimentally, the feasibility of the suggested concept. We also show that our device can be used as a sensor for low frequency vibration detection. In many applications, such as structural health monitoring [32], it is required to detect mechanical vibratory signals at low, down to tens or even few Hz, frequencies. In these applications, spectral signature of a large-scale host structures, such as bridges, [33], wind turbines [34], or airplane wings [35], is monitored in order to detect possible accumulated damage. The use of accelerometers [33] or fiber Bragg grating (FBG) optical sensors [35] is not always convenient since it requires computationally intensive, power-consuming, Fourier processing of the acquired time-history data. On the other hand, the direct frequency detection through resonant operation of micro mechanical filters is challenging due to large mismatch between the acceptable (from the strength point of view) micro devices natural frequencies and the values to be measured. In this context, the ability of the suggested heterodyne device to perform upconversion of the input signal frequency enables detection of the macro-scale structures vibration using miniature low power consumption and low cost MEMS devices, therefore overcoming the inherent frequency mismatch issue.

II. Model

In order to highlight the operational principle of the mechanical superheterodyne and to provide an insight into its dynamic behavior, we first consider the simplest two DOF, mass-spring model of the device, Fig. 1(a),(b). A rigid frame with the central moment of inertia I_F is attached to the vibrating substrate by a massless linearly elastic torsional spring with the stiffness k_θ. The frame performs a tilting motion with the angle $\theta(\hat{t})$, where $\hat{t}$ is time. (Hereafter, hats ($\hat{}$) denote dimensional quantities.) A rigid proof mass M with the central moment of inertia I_M is attached to the frame by a linearly elastic spring with the stiffness k_u. The mass performs a translational motion $\hat{u}(\hat{t})$ within the plane of the frame and the tilting motion together with the frame. For the sake of convenience, the mass and the frame are shown in Fig. 1(a),(b) with a certain vertical offset between them. In the actual device the centroids of the mass and of the frame are located within the same (xy) plane. At this stage, we assume that the geometry is perfectly symmetric and that in the initial undeformed state, the mass centroid C is located at the tilting axis x. The translational vibrations of the mass are excited by an actuating force $\hat{F}(\hat{t})$, which is directed within the plane of the frame. Due to the substrate vibration with the acceleration $\hat{a}(\hat{t})$, the proof mass is also subject to an inertial force with the resultant $M\hat{a}$ acting at the mass centroid C, Fig. 1(b)

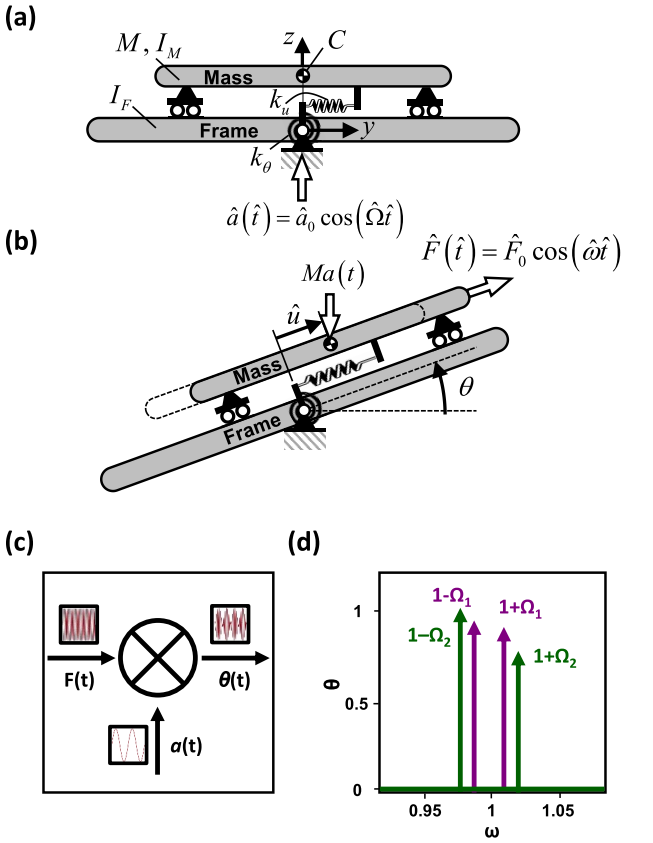

Fig. 1. Lumped two DOF model of the device in the initial unreformed (a) and the deformed (b) configurations. $Ma(t)$ is the resultant of the inertial force acting at the proof mass centroid C. (c) Block diagram of the superheterodyne involving three participating signals (insets): the high frequency actuating force carrier signal $F(t)$ (drive mode), the low frequency input acceleration signal (sense mode) $a(t)$ and the modulated output tilting signal $\theta(t)$. (d) Normalized analytic Fourier Transform of the linearized model solution, Eq. (9), for the normalized (by the tilting mode natural frequency) actuation frequency of $\omega = 1$ and two different non-dimensional substrate acceleration frequencies: $\Omega = \Omega_1 = 0.01$ and $\Omega = \Omega_2 = 0.02$.

The equations of motion are developed using a variational principle (see Supplementary information for details). By substituting the kinetic and the potential energies of the system

$$T = \frac{1}{2}\left(I_F + I_M + M\hat{u}^2\right)\left(\frac{d\theta}{d\hat{t}}\right)^2 + \frac{1}{2}M\left(\frac{d\hat{u}}{d\hat{t}}\right)^2$$
$$U = \frac{1}{2}k_\theta\theta^2 + \frac{1}{2}k_u\hat{u}^2 + M\hat{a}\hat{u}\sin(\theta) - \hat{F}\hat{u} \quad (1)$$

along with the Rayleigh dissipation function $\mathcal{F} = c_\theta(d\theta/d\hat{t})^2/2 + c_u\left(d\hat{u}/d\hat{t}\right)^2/2$, (where c_θ and c_u are the viscous damping coefficients associated with the tilting and the translational motions, respectively) into the Lagrange's equation of the second kind, and assuming $\sin(\theta) \approx \theta$, $\cos(\theta) \approx 1$, we obtain two equations governing the system motion

$$M\frac{d^2\hat{u}}{d\hat{t}^2} + c_u\frac{d\hat{u}}{d\hat{t}} + \left(k_u - M\frac{d\theta}{d\hat{t}}^2\right)\hat{u} + M\hat{a}\theta = \hat{F} \quad (2)$$

$$(I_F + I_M)\frac{d\theta^2}{d\hat{t}^2} + M\frac{d}{d\hat{t}}\left(\hat{u}^2\frac{d\theta}{d\hat{t}}\right) + c_\theta\frac{d\theta}{d\hat{t}} + k_\theta\theta + M\hat{a}\hat{u} = 0 \quad (3)$$

For convenience, we re-write Eqs. (2) and (2) in the non-dimensional form

$$\ddot{u} + \frac{\omega_u}{Q_u}\dot{u} + (\omega_u^2 - \dot{\theta}^2)u + a\theta = F\omega_u^2 \quad (4)$$

$$\frac{d}{dt}\left[(1+u^2)\dot{\theta}\right] + \frac{1}{Q_\theta}\dot{\theta} + \theta + au = 0 \quad (5)$$

where

$$u = \frac{\hat{u}}{r} \quad t = \frac{\hat{t}}{\tau} \quad \omega_u = \frac{\hat{\omega}_u}{\hat{\omega}_\theta}$$
$$Q_u = \frac{\sqrt{k_u M}}{c_u} \quad Q_\theta = \frac{\sqrt{k_\theta(I_F + I_M)}}{c_\theta}$$
$$a = \frac{\hat{a}}{\hat{\omega}_\theta^2 r} \quad F = \frac{\hat{F}}{k_u r} \quad (6)$$

Here $\hat{\omega}_u = \sqrt{k_u/M}$ and $\hat{\omega}_\theta = \sqrt{k_\theta/(I_F + I_M)}$ are, respectively, the translational and the tilting mode natural frequencies corresponding to the linear uncoupled unforced counterparts of Eqs. (4), and (5) (i.e., to the case of $\dot{\theta}^2 = 0$, $F = 0$ in Eq. (4), $u^2 = 0$ in Eq. (5) and $a = 0$ in both equations); Q_u, Q_θ are the corresponding quality factors. In accordance with Eq. (6), the gyration radius $r = \sqrt{(I_F + I_M)/M}$ and the period of the free tilting vibrations $\tau = 1/\hat{\omega}_\theta$ are used as the natural units of the displacement and time, respectively. Hereafter, the overdot denotes derivatives with respect to the non-dimensional time $\dot{(\,)} = d/dt$.

The system Eqs. (4), (5) incorporates both linear and nonlinear coupling between the DOFs. The linear coupling terms are parameterized by the time-dependent substrate acceleration $a(t)$. The nonlinear coupling manifests itself in the centrifugal softening term $\dot{\theta}^2$ in Eq. (4) and in the variable moment of inertia $1 + u^2$ in Eq. (5). Presence of nonlinearities may lead to rich dynamic behavior of the device, while time-dependent coefficients may result in interesting parametric resonant responses [36], [37].

Linearity of the mixing terms au, $a\theta$ offers a possibility to study the heterodyne effect by considering only the linear counterpart of Eqs. (4) and (5). We simplify our model by neglecting $\dot{\theta}^2$ (since $\theta \ll 1$ and $\omega_\theta = 1$) and $a\theta$ in Eq. (4) (since it is small compared to $F\omega_u^2$). In Eq. (5), we assume time-invariant inertia and neglect the $u^2 \ll 1$ term. However, we preserve the inertial coupling in Eq. (5), which is the only driving term exciting the tilting motion.

In the harmonic excitation case $F = F_0\cos(\omega t)$, $a = a_0\cos(\Omega t)$ and the simplified Eqs. (4), (5) are

$$\ddot{u} + \frac{\omega_u}{Q_u}\dot{u} + \omega_u^2 u = F_0\omega_u^2\cos(\omega t) \quad (7)$$

$$\ddot{\theta} + \frac{1}{Q_\theta}\dot{\theta} + \theta = -ua_0\cos(\Omega t) \quad (8)$$

By looking at the Eqs. (7), (8) we may immediately conclude that the mixing takes place and the tilting motion is excited at the frequencies $\omega + \Omega$ and $\omega - \Omega$, as depicted in the schematic block diagram, Fig 1(c). The effect here is a true heterodyne (rather than beats [3]), it is purely geometric and is not influenced by the nature of the actuating force F. By substituting the solution $u(t) = u_0\cos(\omega t - \phi_u)$ of Eq. (7) into Eq. (8) and by solving the resulting equation in terms of θ we obtain the output signal

$$\theta(t) = u_0 a_0\Big[G_1\cos\left((\omega - \Omega)t - \phi_u - \phi_1 - \frac{\pi}{2}\right) + G_2\cos\left((\omega + \Omega)t - \phi_u - \phi_2 - \frac{\pi}{2}\right)\Big] \quad (9)$$

where

$$u_0 = F_0 G_u$$
$$G_u(\omega) = \left[\left(1 - \frac{\omega^2}{\omega_u^2}\right)^2 + \frac{\omega^2}{Q_u^2\omega_u^2}\right]^{-1/2} \quad (10)$$
$$\tan(\phi_u) = \frac{\omega}{Q_u\omega_u}\left[1 - \frac{\omega^2}{\omega_u^2}\right]^{-1}$$
$$G_i(\omega) = \left[\left(1 - \omega_i^2\right)^2 + \frac{\omega_i^2}{Q_\theta^2}\right]^{-1/2}$$
$$\tan(\phi_i) = \frac{\omega_i}{Q_\theta}\left[1 - \omega_i^2\right]^{-1} \quad (11)$$

and $\omega_i = \omega + (-1)^i\Omega$, $(i = 1, 2)$. In accordance with Eqs. (9)-(11), the resonant tilting response occurs at two modulated frequencies $(1 \pm \Omega)\sqrt{1 - 1/(2Q_\theta^2)}$, therefore demonstrating mixing. Moreover, the magnitude of the tilting mode vibrations is linear in terms of the acceleration a_0 and the translational u_0 amplitudes.

Figure 1(d) shows the analytic Fourier transform of the solution, Eqs. (9)-(11). The results correspond to the case of the high frequency translational mode excitation at $\omega_u = 0.85$ and the low frequency inertial excitation at the substrate non-dimensional frequencies of $\Omega = 0.01$ and $\Omega = 0.02$. Two peaks correspond to the non-dimensional driving frequency of $\omega = 1 \pm \Omega$ illustrating the mixing effect. To assure that the solution of the simplified Eqs. (7), (8) is consistent with the results obtained using Eqs. (4), (5), we solved numerically Eqs. (4), (5) and found that for the considered range of parameters, the analytical solution Eq. (9) is in an excellent agreement with the numerical data. It is to say, the influence

of the parametric and nonlinear terms in Eqs. (4), (5) on the mixing effect is minor.

Due to its simplicity and availability of the closed form analytical solution, the lumped model, Eqs. (7), (8) is convenient for the heterodyne effect analysis in the device under consideration. It can be used also at the initial stages of the device development for evaluation of the design parameters. However, our experimental results show additional, not predicted by Eqs. (9)-(11), resonant peaks at certain modulated frequencies. We attribute the presence of these peaks to the influence of the geometric imperfections, which are unavoidable due to the low tolerances of micro machining, and may result in additional dynamic couplings and comb drive related forcing terms.

In order to investigate the influence of the imperfections, we expand the model to include an initial vertical (z-direction) offset $\hat{\delta}$ between the centroid of the mass and the xy plane, (see Fig S.1 in the Supplementary materials). Moreover, in the present work we use an electrostatic force generated by two comb drive transducers to excite the translational motion of the mass. Since the electrostatic force may affect the device's response, our modified model accounts also for the influence of the fringing electrostatic fields, which results in appearance of the time-dependent, parameterized by the voltage, (effective) stiffness coefficients in the governing equations. Note that in the actual device, many other sources of imperfections, such as asymmetry in the mass geometry (resulting in an additional initial in-plane offset) or in the transducers voltages may exist. Since the influence of these imperfections is, at least qualitatively, similar to that of $\hat{\delta}$, we limit our consideration to the case when only the vertical offset is present. After taking into account the influence of imperfections, the following system of equations was obtained (the detailed derivation is found in the Supplementary materials)

$$\ddot{u}+\frac{\omega_u}{Q_u}\dot{u}+(\omega_u^2-\dot{\theta}^2)u+\left[a-\beta\eta\left(y_e+\frac{L_e}{2}\right)(V_R^2+V_L^2)\right]\theta+\delta\ddot{\theta} =\beta h(V_R^2-V_L^2) \quad (12)$$

$$(1+u^2)\ddot{\theta}+2u\dot{u}\dot{\theta}+\frac{1}{Q_\theta}\dot{\theta}+\left[1+\beta\nu L_e y_e^2(V_R^2+V_L^2)\right]\theta +\left[a-\beta\eta\left(y_e+\frac{L_e}{2}\right)(V_R^2+V_L^2)\right]u+\delta\ddot{u} =\beta\eta y_e L_e(V_R^2-V_L^2) \quad (13)$$

Here $\delta=\hat{\delta}/r$ is the normalized vertical offset, η and ν are the non-dimensional parameters associated with the fringing electrostatic fields, L_e is the initial overlap between the comb drive electrodes and y_e is the distance between the midpoint of the electrodes overlap area and the torsion axis x and $h=\hat{h}/r$ is the non-dimensional height of the device, Fig. 2(a). In addition, $\beta=N\varepsilon_0 V_0^2\omega_u^2/(g_0 k_u)$ is the voltage parameter and V_R and V_L are the voltages applied to the right and to the left transducer, respectively. The presence of the $V_R^2+V_L^2=2V_{DC}+V_{AC}(1+\cos(2\omega t))$ terms in Equations (12), (13) may result in parametric excitation of the system. Nonlinear quadratic in u and $\dot{\theta}$ terms may lead to the emergence of additional sidebands peaks in the response spectrum. We emphasize that in accordance with Eq. (13) in our device, in contrast to [31], even in the presence of the actuating force, the desired mixing effect is due to the inertial rather than the electrostatic coupling.

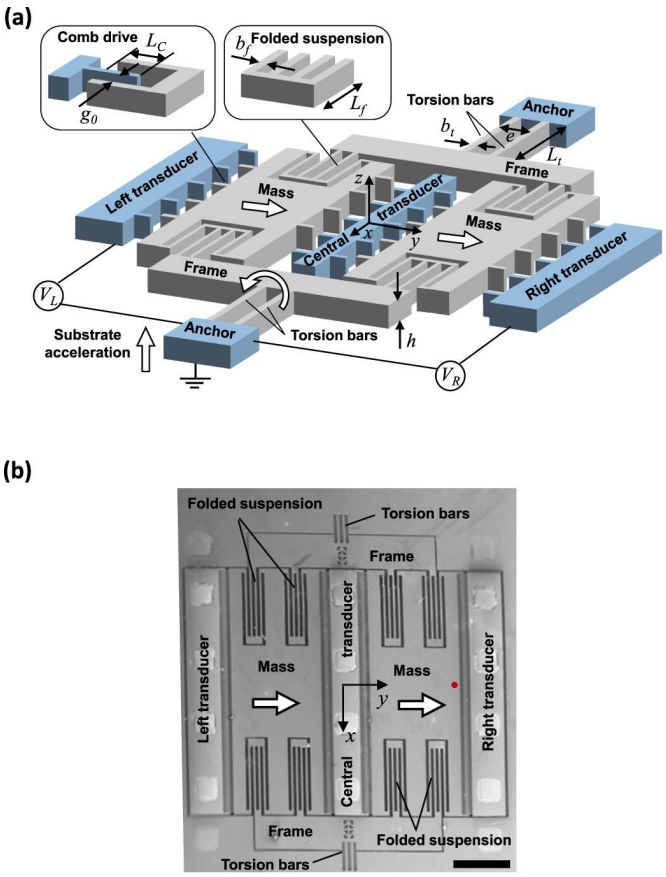

Fig. 2. (a) A schematic view of the device. Elements of the device shown in the gray color are suspended, the parts depicted in the bright blue color are anchored to the substrate. Arrows correspond to the positive directions of motion. (b) Scanning electron micrograph of the fabricated device. The red circle denotes the location where the out-of-plane displacement of the proof mass was measured. The scale bar corresponds to 500 μm.

III. Device Architecture

The device shown in Fig. 2(a) contains a frame performing a tilting motion around the x axis and two identical proof masses designed to move in a translational, in-phase, mode within the plane of the frame (in the y direction) and therefore also undergoing tilting together with the frame. The frame is attached to the unmovable anchors by two double torsion bars. The design based on the double bars allows to increase the in-plane rotational stiffness of the frame suspension. Each of the proof masses is elastically connected to the frame by two folded beam suspensions. The thickness of the device in the out-of-plane z direction is much higher than the width of the folded beams and of the torsion bars. This assures high out-of-plane stiffness of the device. To excite the translational vibrations of the proof mass, we use two comb drive transducers positioned at the outer edges of each of the masses. The third transducer is located at the center of the device, between the two masses. It was not used for actuation in our experiments. The substrate that the entire frame-masses assembly is attached to is forced to vibrate in the out-of-plane z direction.

The devices were fabricated at Rafael Micro Systems center (RAMS) using an in-house wafer level deep reactive ion etching (DRIE) based process (SPTS Pegasus tool) and released by hydrofluoric acid (HF) vapor etching (Primaxx VHF tool). As a starting material, 150 mm highly-doped (P-type Boron, resistivity of 0.01-0.02 Ωcm) SOI wafers with (100) upper surface orientation, 70 μm thick conductive device layer, 2 μm thick buried oxide (BOX) and 400 μm thick conductive handle were used. Metal contact pads were defined by evaporating 0.7 μm thick layer of aluminum. The torsion bars and the folded beams are oriented in the crystallographic <110> direction of Si. The nominal, "as designed", length and width of the torsion bars is $L_t = 340$ μm and $b_t = 25$ μm, respectively, the distance between the centerlines of the double torsion bars is $e = 220$ μm. The length and the width of the folded suspension beams are $L_f = 765$ μm and $b_f = 20$ μm, respectively. Each comb drive actuator contained 149 electrodes, the distance between the electrodes is $g_0 = 5$ μm. The fabricated device, which was used in the experiments, is shown in Fig. 2(b).

IV. Model Results

First, a three-dimensional finite element (FE) model of the device was built (ANSYS package) and four lowest natural frequencies were obtained using the eigenvalue solver (see [48] for details). The model accounts for anisotropy of Si and incorporates actual, measured, geometric parameters of the device, which differ from the nominal values due to fabrication tolerances. The calculated natural frequencies (convergent up to the sub-percent relative error) corresponding to the in-phase translational and tilting modes were $f_u = 4450$ Hz and $f_\theta = 4920$ Hz, respectively. Frequencies corresponding to the undesired anti-phase translational and out-of plane modes were 4594 Hz and 6453 Hz, respectively. The smallest split of 144 Hz was obtained between the in-phase and anti-phase translational modes frequencies. In our experiments, the devices demonstrated quality factors of the order of $Q \approx 2000$. For this reason, the separations between the natural frequencies were sufficient to assure that only the desired vibrational modes are excited. The stiffnesses associated with the in-phase translational and the tilting modes were also calculated and were found to be $k_u = 344$ N/m and $k_\theta = 63.4 \times 10^{-6}$ Nm, respectively. The mass and the combined moment of inertia around the x axis (in the initial undeformed configuration) of the two proof masses system were estimated to be $M_m = 0.440 \times 10^{-6}$ kg and $I_m = 53.110 \times 10^{-15}$ kgm^2, respectively. The frame moment of inertia around the tilting axis was $I_F = 13.240 \times 10^{-15}$kgm^2.

To study the influence of the nonlinear coupling Eqs. (4), (5) completed by zero initial conditions were solved numerically by using the Runge-Kutta-Fehlberg ordinary differential equations solver implemented in Maple. The amplitude of the steady state response was obtained for differing values of the driving frequency ω. Our calculations show that for the adopted realistic device parameters, the results are practically identical to those given by the simplified linear model, Eqs. (7), (8). The calculated peak amplitudes and frequencies differs from the analytically obtained values, Eqs. (9)-(11), by less than 0.001% and 0.01%, respectively.

The influence of imperfections in the device geometry, along with the role of the fringing fields electrostatic force, were explored by numerically solving Eqs. (12), (13). Computation time was chosen to be sufficiently long to eliminate the contribution of the initial conditions and of the transient effects to the high-Q device response. In addition, the FFT of the calculated signal was carried out using only the second part of the time series not affected by the initial conditions. Consistently with our experimental protocols, numerical experiments of two types were carried out. In the first scenario, the inertial carrier signal associated with the substrate acceleration was applied at $\Omega = 1$, which is the tilting mode natural frequency. The translational motion was actuated in a quasi static regime, at $\omega = 0.02 \ll \omega_u$. The result is depicted in Fig. 3(a) where the fast Fourier transform (FFT) of the numerically obtained tilting angle time series is shown. The presence of additional peaks at $\Omega = 1 \pm 3\omega$ is attributed to the influence of nonlinear terms in the system of coupled Eqs. (12), (13). In the second operational scenario, the electrostatic force was applied at $\omega = 0.85$ and served as the carrier signal, while the inertial force was applied at the low frequency of $\Omega = 0.02$. The FFT plot of the tilting angle time series, Fig. 3(b), reveals two peaks at the modulated frequencies $\omega_u \pm \Omega$. The peak at $\omega = 0.85$ is due to the direct forcing term in the right hand side of Eqs. (12), (13).

V. Experiment

A. Experimental Setup

In order to apply an inertial signal, the device was attached to an external piezoelectric actuator Piezostacks PSt1000/16/20VS25 (Piezomechanik GmbH), providing an oscillatory acceleration in the out of plane direction. The actuator was connected to the voltage source through a voltage amplifier (F10A, FLC Electronics). Before running the experiments, we characterized the acceleration signal provided by piezoelectric actuator and found it to be harmonic. The harmonic voltage signal was applied to the left and the right comb drive transducers in such a way that $V_L = V_{DC} + V_{AC}\cos(\hat{\omega}\hat{t})$ and $V_R = V_{DC} - V_{AC}\cos(\hat{\omega}\hat{t})$. The device was placed inside the LCC ceramic package, where the signals were passed to the device through a compatible socket and wirebonding. The piezo actuator with the attached device was mounted on the wafer prober (Karl Suss PM5) equipped with the Mitutoyo FS70 microscope with a 20 ×/WD 20 mm long working distance lens. The prober was mounted on an anti-vibration table (Newport, VH3036). The experiments were conducted at room temperature and under ambient air conditions. The out of plane velocity responses were detected by a laser Doppler vibrometer (Polytec OFV-512), equipped with the OFV5000 controller and VD-02 velocity decoder. During the measurements, the laser spot of the vibrometer was focused at a point located close to the outer edge of the mass where the out-of-plane deflections are maximal (the red point on Fig 1(b)). The vibrometer output was fed into the data acquisition system, which also controlled the input signals. A Polytec PSV8.7 software package was used to manage the

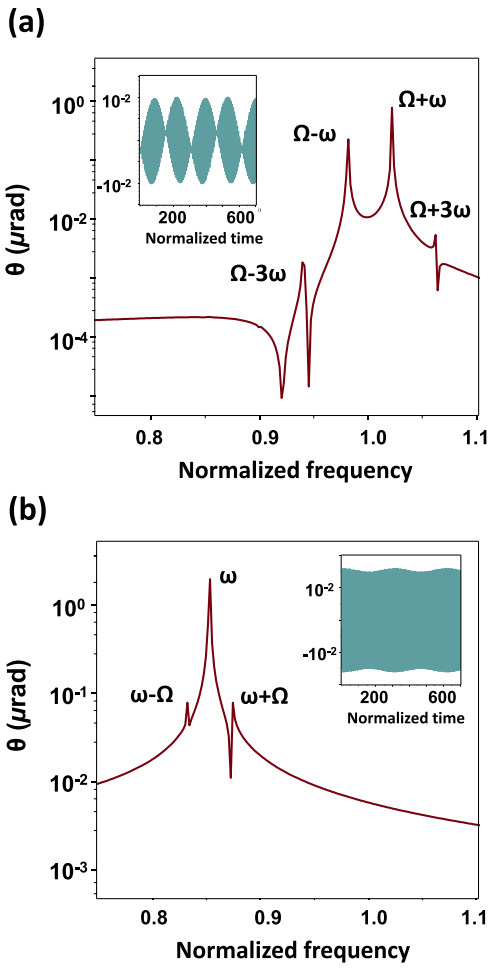

Fig. 3. Model results considering imperfection effects, by meaning of FFT of θ response for (a) inertial input as a carrier ($\Omega \approx 1$) modulated by the electrostatic driving force ($\omega \approx 0.02$), and (b) driving actuation ω as a carrier ($\omega \approx 0.85$) with modulation by low frequency inertial signal ($\Omega \approx 0.02$). Insets show time history for both cases.

measurements and postprocess the results. Time history signals achieved from the vibrometer output were converted into the spectral response of the device.

B. Experimental Results

The goal of the experiments was two fold. The first was to demonstrate the heterodyne effect in the device under consideration and to explore its main features. The second goal was to show that the proposed device can serve as a vibration sensor able to detect frequencies much lower than the device's own natural frequencies. Before carrying out the mixing experiments, the natural frequencies and corresponding quality factors associated with the in-phase translational and the tiling motions were measured. The tilting mode frequency was obtained by applying a transient inertial signal to the device, followed by the FFT of the recorded time series. The in-plane frequency was registered by applying a harmonic voltage to the comb transducer at a wide range of frequencies and using FFT of the measured response to identify the resonant peak. The in-phase translational and tilting frequencies were measured to be ≈4078 Hz and ≈4700 Hz, respectively, and are lower than the corresponding calculated values of 4450 Hz and 4920 Hz. The discrepancy is attributed to the uncertainty in the device geometry, especially in the parameters of the narrow, ≈ 20 μm wide, folded suspension beams and ≈ 25 μm wide torsional bars defining the device stiffness. Due to their small dimensions, these elements are prone to a significant influence of the fabrication-related deviations from the nominal geometry, such as an over etch or side wall angle resulting from the DRIE process. The quality factor associated with the small amplitude tilting motion was measured to be $Q_\theta \approx 2000$, were damping is caused mainly by air damping for small amplitude in free path, and anchor losses.

During our experiments, the devices were operated using two scenarios. In the first case, the acceleration signal was used as a carrier, while the electrostatic force was applied at a low frequency, well below the tilting resonance. The harmonic voltage signal with the amplitude of 50 V and at the frequency of ≈ 4700 Hz was supplied to the shaker. The unipolar harmonic voltage signal with the offset of V_{DC}=15 V, amplitude of V_{AC}=15 V and at the frequencies of 100 Hz, 125 Hz, 150 Hz and 200 Hz was supplied to the comb drive transducers. The frequency responses, in terms of the out-of-plane velocity, are shown in Fig. 4. The presence of the side peaks corresponding to the modulated signals is clearly observed. The presence of the additional side bands in Fig. 4 is attributed to the influence of the nonlinear electrostatic and inertial (centrifugal) coupling between the tilting and the translational motions, nonlinear variable inertia and nonlinearity of the driving electrostatic force. Specifically, since the stationary electrodes of the comb drive transducer are attached to the substrate, the tilting and the translational motions are coupled through the electrostatic force (see Eqs. (S.18), (S.19) in the supplementary materials). This coupling, along with imperfections and the nonlinear variable inertia, Eqs. (12), (13), may result in possibly not purely harmonic frequency translational motion signal $u(t)$. Multiplication of the high frequency harmonic inertial signal $a(t)$ with the non-harmonic $u(t)$ can be seen in Fig. 4. In accordance with Fig. 4 the frequency separations between the adjacent major sidebands are the multipliers of the low frequency signal, implying that the heterodyning affects not only the lowest harmonics but also the sidebands. By subdividing the measured out-of-plane velocities by ω, the peak values amplitudes of the out-of-plane vibrations were estimated to be $\approx$ 0.34 μm for the central resonant peak frequency of ≈ 4700 Hz and ≈ 3.5 nm at the frequencies of the side bands. By further subdividing these values by the distance of ≈ 1400 μm between the measurement point (the red dot in Fig. 2(b)) and the tilting axis, the corresponding angles were ≈ 0.24 mrad and ≈ 2.5 μrad.

In the second vibration sensing experiment, a low frequency inertial force was imposed on the device by the shaker, while the high frequency carrier was provided by the comb drive transducers. The amplitude of the voltage signal supplied to the shaker was 50 V, the frequency varied between 25 Hz and up to 125 Hz with the 25 Hz increments. By measuring the substrate out-of-plane velocities and subdividing the measured values by $\hat{\Omega}$, the resulting accelerations were estimated to be in the range between 1 mg and up to 37 mg. The voltage signal feed

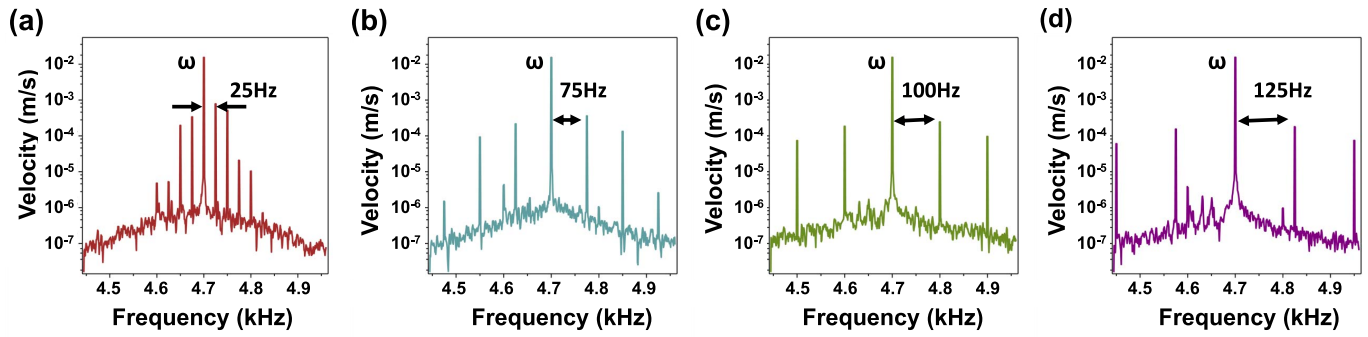

Fig. 4. Experimental tilting response spectrum. The out-of-plane velocity associated with the tilting motion is shown for the constant shaker frequency of ≈ 4700 Hz and different comb drive signal frequencies: (a) ≈ 25 Hz, (b) ≈ 75 Hz, (c) ≈ 100 Hz, and (d) ≈ 125 Hz.

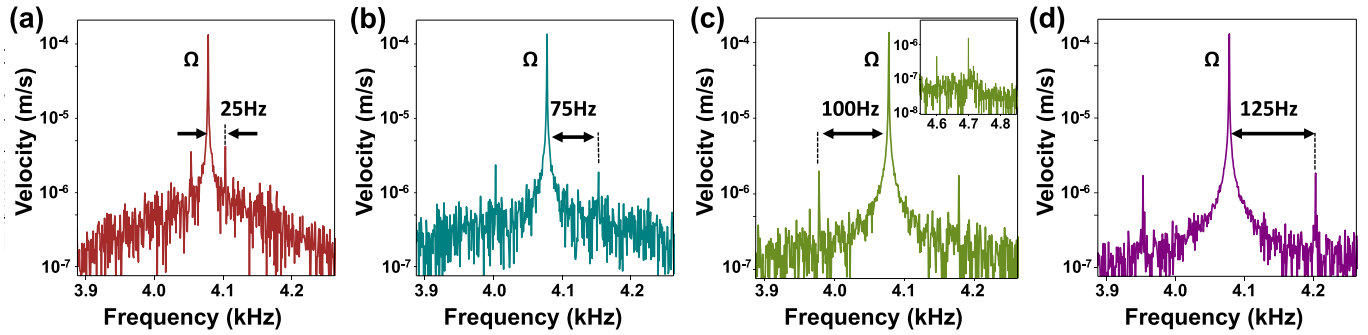

Fig. 5. Experimental tilting response spectrum. The out-of-plane velocity associated with the tilting motion is shown for the constant electrostatic force frequency of ≈ 4078 Hz and different shaker frequencies: (a) ≈ 25 Hz, (b) ≈ 75 Hz, (c) ≈ 100 Hz, and (d) ≈ 125 Hz (d)). Inset in (c) shows the peak in the spectrum corresponding to the in-phase translational mode natural frequency.

into the comb drive transducers was at the resonant frequency ≈ 4078 Hz of the in-phase translational mode. The offset and the amplitude of the signal were $V_{DC} = V_{AC} = 15$ V. The device spectrum shown in Fig. 5 indicates that the frequency intervals separating the sidebands and the carrier peak (corresponding to the tilting mode resonant frequency) are equal to the substrate vibration frequency. In contrast to the case shown in Fig. (4), the low frequency inertial (acceleration) signal is harmonic, the influence of the high-frequency components of the non-harmonic translational response on the mixing is not pronounced and no additional sidebands are observed in Fig. 5. These results, apart from demonstrating the heterodyne effect, suggest that the device can serve as an efficient sensor for detecting a very low frequency of mechanical vibrations. Note that the superheterodyne based detection of the frequencies with the kHz range was reported in [31] and [38]. Here we demonstrate the detection of the much lower frequency of ≈ 25 Hz, which is 0.053% of the tilting mode harmonic.

VI. Discussion

The heterodyne architecture introduced in the present work relies on the inertial coupling between the two vibratory modes of the structure, rather than electrostatic or other nonlinear coupling. In our device, the measured quantity serving as an output is the tilting angle of the proof mass, while the translational motion provides a time-harmonic offset between the tilting axis and the mass centroid, where the inertial force resultant is applied. The frequency multiplying term appears as a product between the inertial force engendered by the vibrating substrate acceleration and the translational displacement. As a result, the mixing term, which is the only term driving the tilting vibrations, is linear in terms of the substrate acceleration and the proof mass displacement. While the influence of nonlinearities on the device response can in principle become more pronounced at higher vibrational amplitudes, the linearity of the mixing term with respect to the substrate acceleration (the input) and the translational displacement is still preserved. The mechanical, geometric, nature of the mixing introduced in this work has several beneficial consequences. In contrast to the electrostatic mixing, our device is not prone to the so called pull-in instability, which often limits the stable amplitude range of the devices. Moreover, since the mixing is mechanical, it is not affected by the nature of the actuating forces driving the proof mass translational vibrations. Despite the fact that electrostatic actuation by a comb drive transducer was implemented in the present work, any other driving mechanism such as magnetic, piezoelectric, or inertial, can be used for this purpose. This expands the design space and offers more freedom in the choice of materials and processing approaches, which can be used for the device fabrication. Apart from the actuation, the mixing itself does not require any electric input (such as voltage or current), which may further reduce power consumption and make the device to be attractive for autonomous

applications. More importantly, the mechanical nature of the mixing makes it invariant to the scale - the device can be up- or downscaled without affecting its functionality. This is in contrast to the heterodyne devices based on the nonlinear electrostatic forces, which generally cannot be scaled up. Note in passing that the same mechanical, based on the inertial coupling, heterodyne concept can be realized in the framework of other architectures. As an example, one can mention an easily down scalable micro or nano cantilever device with a mass elastically attached to the beam and moving along it. From the modeling point of view, the linearity of the mixing term justifies the use of the simplest linear two DOF model, which allows a closed form solution and, despite its simplicity, still predicts heterodyning. The model can be conveniently used for the design purposes, as well as for the analysis of the influence of various design and operation parameters on mixing.

One of the distinguishing features of micromechanical devices is their unique ability to combine sensing and signal processing or logic functions within the same device. This allows significant reduction, or even elimination of a costly and time consuming post processing, and is especially attractive in the scenarios when the sensed signal is of a mechanical character. In this context, the inertial character of the mixing mechanism reported in this work opens interesting possibilities for implementation of the device in various applications. One of the possibilities explored in the present work is the low frequency vibration sensing, which, for example, can be incorporated into structural health monitoring systems. Direct MEMS-based mechanical resonant vibration sensing (mechanical Fourier transform) at the frequencies of the order of several tens or even hundreds of Hz is often challenging, since micro machined devices with such a low natural frequency are too fragile to be practical and are prone to handling-related damages. The use of accelerometers operated in a quasi-static mode requires complex processing of the time-series data and is not always suitable. Here we show both experimentally and by using the model, that the device can be applied for ultra low frequency vibration sensing. Substrate vibrations at the frequency as low as $\approx$ 25 Hz were measured using a robust and manufacturable device with the natural frequency as high as $\approx$ 4700 Hz. The minimal detectable frequency and the frequency resolution can be improved by operating the device at higher quality factors using appropriate packaging. We emphasize that in our experiments the device was actually operated as a superheterodyne when the input signal (substrate vibrations) frequencies were up-converted to the fixed intermediate frequency, namely the natural frequency associated with the tilting mode. The proof mass vibrating in the translational mode served as a local oscillator. It should be mentioned that while our calculations and experiments were carried out for the signals close to one of the natural frequencies of the system the heterodyne effect is possible at any combination of the inertial and the driving signal frequencies. However, for the energetic efficiency considerations, it is preferable to exploit the resonant amplification of the device response. This is especially suitable for micro- and nanomechanical resonant devices, which could demonstrate extremely high quality factors [6]–[9].

The mechanical mixing paradigm introduced here can be also exploited in other sensors. For example, the same measurement concept, which was used for the frequency measurement of the vibrating substrate, can be directly used for the spectral analysis of other forces, such as acoustic or electromagnetic, or even van der Walls forces in atomic force microscope (AFM). The device, with certain design modifications, can be used as a pressure sensor, microphone, electric/magnetic field sensor or even for speech recognition [39]. In all these implementations, the product of a time-harmonic force (of any kind) and of the proof mass displacement will result in a heterodyne effect and in the resonant excitation of the tilting vibrations. The device can also be used as a resonant accelerometer operated in the frequency monitoring scenario. For example, in the case of $a = const$, the eigenvalues of the linear undamped and unforced counterpart of Eqs. (4) and (5) $\lambda_{1,2} = (\omega_u^2 + 1 \pm \sqrt{(\omega_u^2 - 1)^2 + 4a^2})/2$ are parameterized by the acceleration, which can be extracted from the resonance frequencies measurements. In addition to sensing applications, the ability of the mechanical superheterodyne to convert low frequency, broad band, signals into high frequency resonant oscillations of the tilting mode is a beneficial feature in the field of energy harvesters [40]. Linearity of the mixing term in acceleration is especially attractive in this case, since the device can be operated at high substrate accelerations and therefore at high input powers.

To summarize, we believe that the architecture and the operational concept of the purely mechanical and therefore scalable, reliable and manufacturable heterodyne presented in this work, opens new intriguing possibilities in the realm of micro and nano mechanical signal processing devices, and may lead to better and more efficient designs of these systems and their implementation in new applications.

REFERENCES

[1] D. F. Elliott, *Handbook of Digital Signal Processing: Engineering Applications*. Amsterdam, The Netherlands: Elsevier, 2013.

[2] K. Kikuchi, "Fundamentals of coherent optical fiber communications," *J. Light. Technol.*, vol. 34, no. 1, pp. 157–179, Jan. 1, 2016.

[3] G. Verbiest and M. Rost, "Beating beats mixing in heterodyne detection schemes," *Nature Commun.*, vol. 6, p. 6444, Mar. 2015.

[4] F. Yang, A. Tashchilina, E. S. Moiseev, C. Simon, and A. I. Lvovsky, "Far-field linear optical superresolution via heterodyne detection in a higher-order local oscillator mode," *Optica*, vol. 3, no. 10, pp. 1148–1152, 2016.

[5] B. Liebowitz, "The theory of heterodyne receivers," *Proc. Inst. Radio Eng.*, vol. 3, no. 2, pp. 185–194, Jun. 1915.

[6] G. K. Ho, R. Abdolvand, and F. Ayazi, "Through-support-coupled micromechanical filter array," in *Proc. IEEE Int. Conf. Micro Electro Mech. Syst. (MEMS)*, Jan. 2004, pp. 769–772.

[7] M. A. A. Hafiz, L. Kosuru, M. I. Younis, and H. Fariborzi, "A 2:1 MUX based on multiple MEMS resonators," *Procedia Eng.*, vol. 168, pp. 1642–1645, Sep. 2016.

[8] G. Piazza, P. J. Stephanou, and A. P. Pisano, "One and two port piezoelectric higher order contour-mode MEMS resonators for mechanical signal processing," *Solid-State Electron.*, vol. 51, nos. 11–12, pp. 1596–1608, 2007.

[9] C. T.-C. Nguyen, "MEMS technology for timing and frequency control," *IEEE Trans. Ultrason., Ferroelectr., Freq. Control*, vol. 54, no. 2, pp. 251–270, Feb. 2007.

[10] B. Charlot, W. Sun, K. Yamashita, H. Fujita, and H. Toshiyoshi, "Bistable nanowire for micromechanical memory," *J. Micromech. Microeng.*, vol. 18, no. 4, 2008, Art. no. 045005.

[11] I. Mahboob, E. Flurin, K. Nishiguchi, A. Fujiwara, and H. Yamaguchi, "Interconnect-free parallel logic circuits in a single mechanical resonator," *Nature Commun.*, vol. 2, pp. 197–198, Feb. 2011.
[12] M. A. A. Hafiz, L. Kosuru, and M. I. Younis, "Microelectromechanical reprogrammable logic device," *Nature Commun.*, vol. 7, p. 11137, Mar. 2016.
[13] D. Weinstein and S. A. Bhave, "The resonant body transistor," *Nano Lett.*, vol. 10, no. 4, pp. 1234–1237, 2010.
[14] R. A. Coutu, R. A. Coutu, Jr., and J. W. McBride, "A review of microcontact physics for microelectromechanical systems (MEMS) metal contact switches," *J. Micromech. Microeng.*, vol. 23, no. 10, 2013, Art. no. 103001.
[15] V. Maiwald *et al.*, "Experimental fractal-like instability bands in a resonant silicon-silicon contact pull-in vibration detector," in *Proc. IEEE Int. Conf. Micro Electro Mech. Syst. (MEMS)*, Jan. 2018, pp. 984–987.
[16] L. Hall, "Automaton rover for extreme environments nasa innovative advanced concepts (NIAC) phase I final report," NASA, Washington, DC, USA, Tech. Rep. HQ-E-DAA-TN39181, 2017.
[17] A. B. Clymer, "The mechanical analog computers of Hannibal Ford and William Newell," *IEEE Ann. Hist. Comput.*, vol. 15, no. 2, pp. 19–34, 1993.
[18] Y. Tsividis, "Not your Father's analog computer," *IEEE Spectr.*, vol. 55, no. 2, pp. 38–43, Feb. 2018.
[19] J.-S. Wenzler, T. Dunn, T. Toffoli, and P. Mohanty, "A nanomechanical Fredkin gate," *Nano Lett.*, vol. 14, no. 1, pp. 89–93, Dec. 2014.
[20] J. R. Baitteinger, "Mechanical heterodyne oscillator," U.S. Patent 3 344 873 A, Mar. 10, 1967.
[21] A.-C. Wong and C. T.-C. Nguyen, "Micromechanical mixer-filters ('mixlers')," *J. Microelectromech. Syst.*, vol. 13, pp. 100–112, Feb. 2004.
[22] A. A. Chandran and M. I. Younis, "Multi frequency excited MEMS cantilever beam resonator for Mixer-Filter applications," in *Proc. 3rd Int. Conf. Signal Process. Integr. Netw. (SPIN)*, Feb. 2016, pp. 735–742.
[23] M. Koskenvuori and I. Tittonen, "Parametrically amplified microelectromechanical mixer," in *Proc. IEEE 21st Int. Conf. Micro Electro Mech. Syst. (MEMS)*, Jan. 2008, pp. 1044–1047.
[24] S. Ilyas, N. Jaber, and M. I. Younis, "MEMS logic using mixed-frequency excitation," *J. Microelectromech. Syst.*, vol. 26, pp. 1140–1146, Oct. 2017.
[25] S.-R. Chung, S. Park, E. M. Abdel-Rahman, J. T. W. Yeow, and M. Khater, "Architecture for MEMS-based analogue demodulation," *J. Microelectromech. Syst.*, vol. 23, no. 4, 2013, Art. no. 045013.
[26] A. Uranga *et al.*, "Fully integrated MIXLER based on VHF CMOS-MEMS clamped-clamped beam resonator," *Electron. Lett.*, vol. 43, no. 8, pp. 452–453, 2007.
[27] V. Sazonova, Y. Yalsh, I. Üstuñel, D. Roundy, T. A. Arlas, and P. L. McEuen, "A tunable carbon nanotube electrochemical oscillator," *Nature*, vol. 431, no. 7006, pp. 284–287, 2004.
[28] R. B. Reichenbach *et al.*, "Third-order intermodulation in a micromechanical thermal mixer," *J. Microelectromech. Syst.*, vol. 14, no. 6, pp. 1244–1252, Dec. 2005.
[29] L. Sekaric, M. Zalalutdinov, S. W. Turner, A. T. Zehnder, J. M. Parpia, and H. G. Craighead, "Nanomechanical resonant structures as tunable passive modulators of light," *Appl. Phys. Lett.*, vol. 80, no. 19, pp. 3617–3619, 2002.
[30] D. Scheibner, J. Wibbeler, J. Mehner, B. Brämer, T. Gessner, and W. Dötzel, "A frequency selective silicon vibration sensor with direct electrostatic stiffness modulation," *Analog Integr. Circuits Signal Process.*, vol. 37, no. 1, pp. 35–43, 2003.
[31] R. Forke, D. Scheibner, K. Hiller, T. Gessner, and W. Dötzel, and J. Mehner, "Fabrication and characterization of a force coupled sensor–actuator system for adjustable resonant low frequency vibration detection," *Sens. Actuators A, Phys.*, vols. 145–146, pp. 245–256, Jul./Aug. 2008.
[32] D. Balageas, C.-P. Fritzen, and A. Güemes, *Structural Health Monitoring*, vol. 90. Hoboken, NJ, USA: Wiley, 2010.
[33] F. Magalhães, A. Cunha, and E. Caetano, "Vibration based structural health monitoring of an arch bridge: From automated OMA to damage detection," *Mech. Syst. Signal Process.*, vol. 28, pp. 212–228, Apr. 2012.
[34] C. C. Ciang, J.-R. Lee, and H.-J. Bang, "Structural health monitoring for a wind turbine system: A review of damage detection methods," *Meas. Sci. Technol.*, vol. 19, no. 12, 2008, Art. no. 122001.
[35] H. Guo, G. Xiao, N. Mrad, and J. P. Yao, "Fiber optic sensors for structural health monitoring of air platforms," *Sensors*, vol. 11, no. 4, pp. 3687–3705, Mar. 2011.
[36] M. Pirmoradian and H. Karimpour, "Parametric resonance and jump analysis of a beam subjected to periodic mass transition," *Nonlinear Dyn.*, vol. 89, no. 3, pp. 2141–2154, 2017.
[37] S. Krylov, K. Lurie, and A. Ya'akobovitz, "Compliant structures with time-varying moment of inertia and non-zero averaged momentum and their application in angular rate microsensors," *J. Sound Vib.*, vol. 330, pp. 4875–4895, Sep. 2011.
[38] R. Forke, D. Scheibner, J. Mehner, T. Gessner, and W. Dotzel, "Adjustable force coupled sensor-actuator system for low frequency resonant vibration detection," in *Proc. Int. Solid-State Sensors, Actuat. Microsyst. Conf. (TRANSDUCERS)*, Jun. 2007, pp. 1725–1728.
[39] D. Haronian and N. C. MacDonald, "A microelectromechanics-based frequency-signature sensor," *Sens. Actuators A, Phys.*, vol. 53, nos. 1–3, pp. 288–298, 1996.
[40] S. Beeby, M. J. Tudor, and N. M. White, "Energy harvesting vibration sources for microsystems applications," *Meas. Sci. Technol.*, vol. 17, no. 12, pp. R175–R195, 2006.

Naftaly Krakover received the B.Sc. and M.Sc. degrees in mechanical engineering from Tel Aviv University, in 2013 and 2014, respectively, where he is currently pursuing the Ph.D. degree in mechanical engineering with the School of Mechanical Engineering, under the supervision of Prof. S. Krylov. His Ph.D. research is focused on MEMS design, especially inertial sensors, frequency-based micro sensors, resonators, and vibration sensing.

Ronen Maimon received the B.Sc. and M.Sc. degrees in mechanical engineering from the Technion Israel Institute of Technology, in 1998 and in 2001, respectively. He is currently pursuing the a Ph.D. degree under the supervision of Prof. S. Krylov with Tel Aviv University. He is currently a Research Associate with Rafael Advanced Defense Systems Ltd. His main research interests include inertial MEMS, design, and dynamics.

Tamar Tepper-Faran received the B.A. degree in physics from Technion in 1994, and the B.Sc., M.Sc., and Ph.D. degrees in materials science and engineering from Technion, Israel, in 1994, 1997, and 2000, respectively. From 2001 to 2002, she was a Fulbright Post-Doctoral Fellow, Department of Materials Science and Engineering, MIT, in the field of magneto-optic thin films. Since 2003, she has been with Rafael Advanced Defense Systems Ltd. As a Senior Process Engineer and as a Research field of MEMS processing and technologies. Her research focused on thin films and nano-structured materials. Her main interest fields are the dry etching of silicon and the Associate in the design for manufacturability.

Yuval Gerson received the B.Sc., M.Sc., and Ph.D. degrees in mechanical engineering from the School of Mechanical Engineering with Tel Aviv University, in 2000, 2008, and 2016, respectively. His research interests are focused on meso-scale and large displacements MEMS actuators and sensors. From 2010 to 2015, he was an Expert Consultant with Rafael Advanced Defense Systems Ltd.

Richard Rand is currently a Professor with the MAE Department and the Math Department with Cornell University. His research interests involve by using perturbation methods and bifurcation theory to obtain approximate solutions to differential equations arising from nonlinear dynamics problems in engineering and biology. His current projects involve differential equations with delay terms and include the applications to MEMS and to queuing theory.

Slava Krylov received the M.Sc. and Ph.D. degrees in applied mechanics from the State Marine Technical University of St. Petersburg, Russia, in 1989 and 1993, respectively. He was a Visiting Professor with the School of Applied and Engineering Physics and Mary Shepard B. Upson Visiting Professor with The Sibley School of Mechanical and Aerospace Engineering, Cornell University, and also a Visiting Researcher with the Center for the Nanoscale Science and Technology (CNST), The National Institute of Standards and Technology (NIST), Gaithersburg, MD, USA. From 1994 to 2002, he was a Colton Post-Doctoral Fellow at the Department of Solid Mechanics, Materials and Systems, Tel Aviv University, where he was with Israel Aircraft Industries, and then as a Principal Scientist and the Co-Founder of a start-up company developing optical MEMS. He joined the School of Mechanical Engineering, Tel Aviv University, as a Faculty Member, in 2002, where he is currently a Professor and The Henry and Dinah Krongold Chair of microelectronics. His research interest focuses in the areas of design and modeling of micro- and nanoelectromechanical systems, dynamics and stability of micro- and nanoelectromechanical devices, micro actuators, inertial and flow sensors, nano resonators for bio sensing applications, and optical MEMS. He was the General Co-Chair of the 11th Micro Nano Systems Conference from the ASME IDETC/CIE Conferences 2017, Cleveland, OH, USA.